Bachelor's Thesis
Bachelor's Programme in Physical Sciences
Astronomy

Accuracy of Shock Normal Vectors Measured by Solar Orbiter

Antti Kukkola

June 21, 2022

Supervisor: Dr. Andreas Johlander
Swedish Institute of Space Physics

Examiner: Dr. Markus Battarbee

University of Helsinki
Faculty of Science

PL 64 (Gustaf Hällströmin katu 2a)
00014 University of Helsinki

HELSINGIN YLIOPISTO — HELSINGFORS UNIVERSITET — UNIVERSITY OF HELSINKI

Tiedekunta — Fakultet — Faculty	Koulutusohjelma — Utbildningsprogram — Degree programme
Faculty of Science	Bachelor's Programme in Physical Sciences Astronomy

Tekijä — Författare — Author

Antti Kukkola

Työn nimi — Arbetets titel — Title

Accuracy of Shock Normal Vectors Measured by Solar Orbiter

Työn laji — Arbetets art — Level	Aika — Datum — Month and year	Sivumäärä — Sidantal — Number of pages
Bachelor's Thesis	June 21, 2022	27

Tiivistelmä — Referat — Abstract

Aurinkokuntamme keskellä pääsarjaan kuuluva tähti Aurinko syöksee jatkuvasti varautuneita hiukkasia ympäröivään avaruuteen täyttäen aurinkokunnan. Nämä hiukkaset ovat plasmaa, jota kutsutaan aurinkotuuleksi. Auringon aktiivisuudesta johtuen aurinkotuulen nopeus vaihtelee. Kun aurinkotuuli kohtaa esteen, kuten Maan magneettikentän, tai ohittaa hitaampaa aurinkotuulta, voi syntyä šokkiaalto, jossa plasman tiheys, paine ja lämpötila nousevat äkisti. Tämän työn aiheena on planeettojen väliset šokkiaallot, joita syntyy esimerkiksi auringonpurkauksien seurauksena. Planeettojen väliset šhokkiaallot voivat joissain tapauksissa kiihdyttää hiukkasia niin suuriin nopeuksiin, että ne aiheuttavat vaaraa ihmisille ja avaruusluotaimille maan magneettikentän ulkopuolella. Tämän prosessin tehokkuus riippuu šokkiaaltojen geometriasta, jota tutkimme tässä työssä.

Šokkiaaltojen geometriassa tärkeä parametri on niiden normaalivektori, joka on šhokkiaallon pintaa vasten kohtisuorassa oleva vektori. Tämän selvittäminen planeettojen välisille šokkiaalloille voi olla haastavaa, sillä siihen tarvitaan tarkkoja avaruusluotainmittauksia. Tässä työssä mittaamme normaalivektorit monesta Solar Orbiter -avaruusluotaimen havaitsemasta šokkiaaltotapahtumasta. Solar Orbiter on vuonna 2020 laukaistu eurooppalainen luotain, joka tutkii Aurinkoa ja aurinkotuulta. Käytämme normaalivektorin selvittämiseen useita menetelmiä, joista osa tarvitsee mittauksia aurinkotuulen ominaisuuksista ja osa vain magneettikentästä.

Tutkimuksessamme paljastui, että pelkästään magneettikenttää käyttävät metodit tuottavat jopa $30° - 50°$ aurinkotuulen ominaisuuksia hyödyntävistä metodeista eroavia normaalivektoreita. Validoimme tuloksemme käyttäen Nasan Magnetospheric Multiscale -tehtävää (MMS), joka koostuu monesta luotaimesta ja pystyy niitä hyödyntäen määrittämään šokkiaallon normaalivektorin suurella tarkkuudella. Aurinkotuulen ominaisuuksia hyödyntävät metodit erosivat MMS:n normaalivektorista noin $5°$, kun taas magneettikenttä metodit erosivat enemmän. Johtopäätöksemme on, että on mahdotonta selvittää planeettojen välisen šokkiaallon normaalivektori käyttäen vain magneettikentän mittauksia.

Avainsanat — Nyckelord — Keywords

Shocks, Solar wind, Solar Orbiter

Säilytyspaikka — Förvaringsställe — Where deposited

Muita tietoja — Övriga uppgifter — Additional information

Contents

Abstract in English **1**

1 Introduction **3**
1.1 The Sun and heliosphere 3
1.2 Interplanetary shocks 5

2 Solar Orbiter **7**
2.1 Spacecraft & mission 7
2.1.1 MAG 8
2.1.2 SWA 8
2.2 Events 9

3 Solar Orbiter shock crossings **11**
3.1 Normal vector of an interplanetary shock 11
3.2 Comparing all events 14

4 MMS event **17**

5 Conclusions **21**

Acknowledgements **22**

Appendix A Shock normal vectors for all Solar Orbiter events **23**

Bibliography **25**

Abstract in English

At the center of our solar system a main sequence star called the Sun constantly blows charged particles into the surrounding space, filling the solar system. These charged particles are plasma known as the solar wind. The activity of the Sun causes the solar wind to have varying flow speeds. When the solar wind encounters an obstacle such as Earth's magnetic field or overtakes slower moving solar wind, a shock wave may form, where the density, pressure and temperature of the plasma are suddenly increased. This work is about interplanetary shocks, which form for example after solar eruptions. Interplanetary shocks can accelerate particles to high enough velocities that they became dangerous for humans and spacecraft outside Earth's protective bubble, the magnetosphere. How effectively particles are accelerated in interplanetary shocks depends on the shock geometry, which we will study in this work.

An important parameter of the shock geometry is the shock normal vector, which is a vector perpendicular to the shock surface. Measuring the normal vector is a difficult task that relies on accurate spacecraft measurements of the shock. In this work we determine the shock normal vector from multiple shock events using Solar Orbiter, a newly launched European spacecraft investigating the Sun and the solar wind. We use multiple methods, some of which use measurements of solar wind properties and some that only require magnetic field data.

We find that the magnetic field methods produce normal vectors that deviate significantly, up to $30-50$ degrees, from those determined by methods using solar wind properties in addition. We validate our results using Magnetospheric Multiscale mission (MMS) which is a NASA multi-spacecraft mission that can determine the shock normal with greater accuracy with multiple shock crossing measurements. We find that the methods using solar wind properties are about 5° off of the normal vector measured by MMS while the magnetic field methods again produce normal vectors that deviate more. We conclude that it is impossible to determine the shock angle for an interplanetary shock using only magnetic field measurements.

1. Introduction

1.1 The Sun and heliosphere

The Earth revolves around a main sequence star, the Sun. In its core, energy is continuously produced by nuclear fusion. This energy is transported to the surface of the Sun through a radiation zone and through a convection zone further from the core [Guenther et al., 1992]. The energy radiates from the Sun to the nearby space reaching, among other planets, Earth and sustaining all life. From the Earth, the Sun's photosphere is the most apparent layer, however during a solar eclipse, when the Moon blocks the Sun, a further layer called the corona is visible. The Sun in ultraviolet wavelength is shown in Figure 1.1a and the corona, imaged during a solar eclipse, is shown in Figure 1.1b.

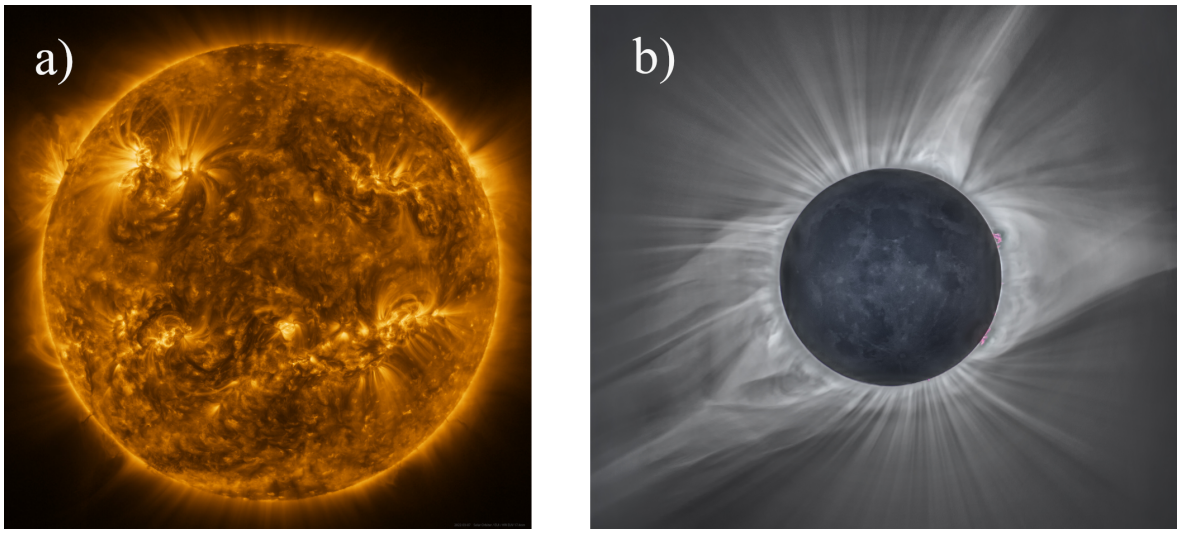

Figure 1.1: Left panel: The Sun as seen by solar orbiter in ultraviolet wavelength. Image credit: ESA & NASA/Solar Orbiter/EUI team. Right panel: Composite image generated from photograph of a total solar eclipse. Image credit: Michael S Adler (CC BY-SA 4.0).

From the corona, a stream of charged particles flows outwards filling the solar system. The flow of particles is a plasma known as the solar wind. Plasma is a state of matter consisting of positively and negatively charged particles forming a

quasi-neutral gas that is subject to electromagnetic and other forces. Plasma is highly electrically conductive, which can force magnetic field lines to be frozen-in with the plasma constraining the field lines to move with it. In the case of the solar wind, the interplanetary magnetic field (IMF), originating from the Sun, is frozen-in and therefore embedded in it.

The solar wind flows through the solar system with supersonic speeds, forming a cavity in the interstellar medium. This, roughly bubble-shaped cavity is the furthest layer of the Sun's atmosphere, called the heliosphere [Schwenn and Marsch, 1990]. Eventually as the solar wind flows beyond the orbits of the planets, it slows down from supersonic to subsonic speeds forming a termination shock, which has been observed by the Voyager missions [Krimigis et al., 2003; Burlaga et al., 2009]. Past the termination shock, the solar wind continues to slow down in the so-called heliosheath until the pressures of the interstellar medium and the solar wind balance out in a region called the heliopause, which is the outer border of the heliosphere.

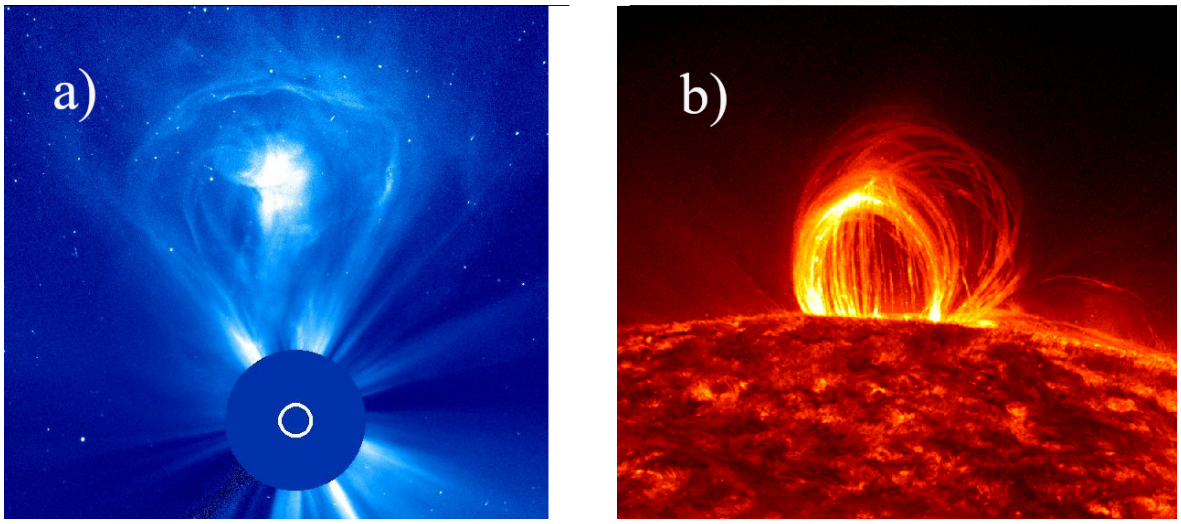

Figure 1.2: Left panel: Coronal mass ejection. Image credit: SoHO/LASCO/ESA/NASA. Right panel: Plasma falling back to the Sun along magnetic field lines as Coronal rain. Pictured at ultraviolet wavelength of 304 angstrom. Image credit: NASA/GSFC/SDO.

The shape of the heliosphere is affected by the interstellar medium and the motion of the solar system through it, but even more so by the solar wind as it changes in much shorter timescales, from hours to years. The Sun's activity causes changes in the solar wind. Coronal mass ejections (CME) are events in which significant amount of coronal plasma is ejected into the interplanetary space as solar wind. On Earth, CMEs cause geomagnetic storms and auroras as the particles and electromagnetic field in the CME interact with Earth's magnetic field. The frequency of CMEs changes according to the solar cycle, a 11 year long periodic change in the activity of the Sun. During the solar maximum multiple CMEs can occur during a day whereas during the solar

minima only a few CMEs happen within a week [Schwenn and Marsch, 1990]. A CME is shown in Figure 1.2a. An aftermath of a CME where plasma from the corona is falling down towards the surface of the Sun along the magnetic field lines is shown in Figure 1.2b.

1.2 Interplanetary shocks

Variations of the solar wind speed cause faster solar wind to overtake slower moving solar wind which may form shocks in the overlap regions. A common example for this is coronal mass ejections where a shock forms ahead of the ejected plasma if the speed difference to the local solar wind speed is large enough [Miralles and Sánchez Almeida, 2011]. Another type of interplanetary shock can form in corotating interaction regions (CIR) where plasma from faster solar wind stream catches up with a slower stream. The solar wind streams are twisted to spiral shapes by the rotation of the Sun making CIRs also have a spiral shape. A pair of shocks form in the borders of CIRs with a discontinuity region between the two [Schwenn and Marsch, 1990].

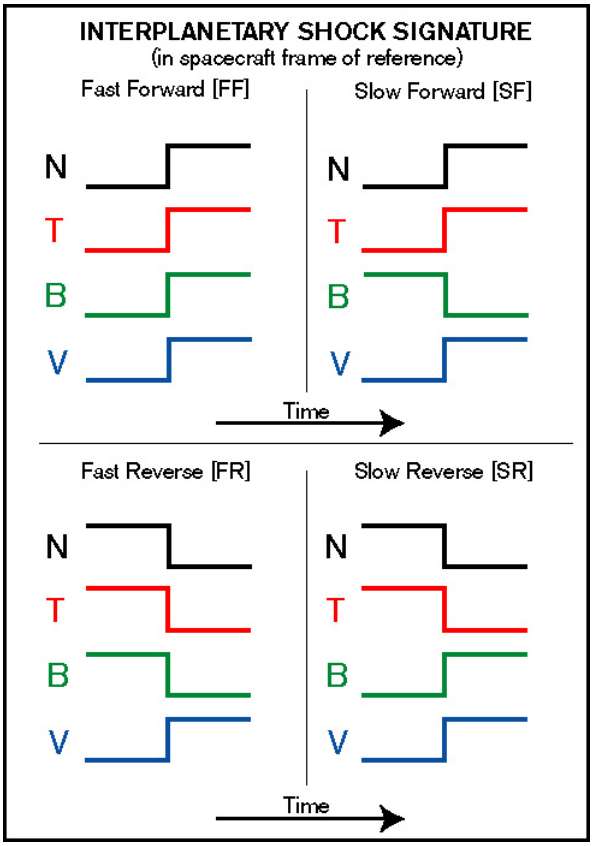

Figure 1.3: The four types of interplanetary shocks. Image credit: NASA/WIND/MFI

There are two main types of interplanetary shocks: fast shocks where the shocked plasma has increased magnetic field, and slow shocks with decreased magnetic field.

Both types heat up the solar wind plasma. Additionally, in the solar wind frame of reference, the shock can move away from the Sun, making it a forward shock, or towards the Sun making it a reverse shock [Burlaga, 1995]. Since the solar wind is supersonic, both forward and reverse shocks move away from the Sun in the in the frame of reference of the Sun, the Earth or a spacecraft. The signatures of these four types of shocks are shown in Figure 1.3. The most commonly observed type of interplanetary shock is the fast forward shock, hence it is the only type that is used in this work.

Interplanetary shocks are a great laboratory for astrophysical shocks in general as they share mechanisms with more energetic shocks such as those in gamma ray bursts and supernova remnants where particles are accelerated to very high velocities becoming cosmic rays. Interplanetary shocks can also accelerate particles to very high velocities in CME shocks. These solar energetic particles (SEP) can be energetic enough to cause danger to humans and spacecraft during space flight. An important parameter in shocks for the origins of SEPs, and shocks in general, is the angle between the shock normal vector $\hat{\mathbf{n}}$ and the interplanetary magnetic field θ_{Bn} as the incoming ions behave differently whether they encounter a shock that is parallel or perpendicular to the magnetic field. To calculate θ_{Bn} we of course must know $\hat{\mathbf{n}}$. The purpose of this study is to test different methods for determining $\hat{\mathbf{n}}$ from spacecraft observations and comparing them with each other to see how to accurately calculate the shock angle.

2. Solar Orbiter

2.1 Spacecraft & mission

Figure 2.1: Artist's rendering of the Solar Orbiter. Image credit: ESA.

Solar Orbiter (SolO) is a spacecraft mission by the European Space Agency with collaboration from NASA, which aims to study the Sun and heliosphere [Müller et al., 2020]. The SolO mission will answer fundamental science problems such as questions regarding origins of the solar wind, origins and evolution of coronal mass ejections (CME) and the nature of solar energetic particles. While previous missions (e.g., Helios [Porsche, 1981] and Ulysses [Wenzel et al., 1992]) have provided much valuable information on the Sun, heliosphere and space physics itself, the SolO mission will shed light on two not yet fully explored areas: the inner heliosphere and the Sun's polar

regions. The spacecraft was launched in February 2020 and has a nominal mission of 7 years during which it will have a close encounter ($\sim$ 0.3 AU) with the Sun every 6 months.

The Solar Orbiter spacecraft is stabilized along three axes and is built around a central cylinder pointed towards the Sun with a heat shield in front to protect the spacecraft from the solar flux. The spacecraft can be seen in Figure 2.1. The spacecraft has two solar arrays on its sides making its wingspan 18 meters when deployed. Solar Orbiter has 10 instruments consisting of both remote-sensing and in-situ instruments. The orbit of the spacecraft will be clearly out of the ecliptic plane owing to several gravitational assist maneuvers with Venus and Earth. This combined with both in-situ and remote-sensing instruments distinguishes it from previous missions.

We will next look at a few Solar Orbiter instruments important for this work.

2.1.1 MAG

The Solar Orbiter has a dual sensor fluxgate magnetometer (MAG) that continuously provides in-situ measurements of the heliospheric magnetic field during the Solar Orbiter mission [Horbury et al., 2020]. The precision of the instrument is $\sim$ 5 pT making it possible to detect the largest scale magnetic field changes as well as those below the scale of the proton gyroradius. The magnetometer can operate and measure in multiple time resolutions: up to 16 samples/s in its "normal" mode and 128 samples/s in burst mode. The data used in this work has a sample rate of 8 samples/s. The instrument contributes to many science questions of the mission and is important in the detection of heliospheric shock waves.

2.1.2 SWA

The Solar Wind Analyser (SWA) is a suite of sensors measuring and categorizing ions and electrons in the solar wind. SWA also measures the abundances and charge states of heavy ion populations [Owen et al., 2020]. This fully characterizes the solar wind in the operating region of the spacecraft in the inner heliosphere, and provides 3D velocity distribution functions (VDF) for the solar wind for both electrons and ions as well as alpha particles. The three sensors that make up SWA are the Electron Analyser System (SWA/EAS), the Proton and Alpha Particle Sensor (SWA/PAS) and the Heavy Ion Sensor (SWA/HIS). Data from all sensors is processed in the central Data Processing Unit (SWA/DPU).

The most important sensor in SWA for this work is the SWA/PAS. It has a single electrostatic analyser head with a cut-out in the heat shield to allow solar wind ions to reach the sensor aperture. Multiple aperture deflection plates steer the ions in to

the detector while sunlight passes through the aperture. SWA/PAS can produce a statistically valid 3D ion VDF every 4 seconds at a distance of 1 AU to the Sun, with the rate increasing closer to the Sun. The time resolution for the data in this work is generally 4 s.

2.2 Events

A year in to its flight, the Solar Orbiter has already encountered numerous heliopheric shock waves. The dates of the events used in this work are listed in Table 2.1. All of the events are fast forward type shocks. While the cause of the shocks is not known, we can suspect they are CME shocks as they are the most common type of interplanetary shock [Richardson, 2011]. All the events were identified before this work. The five shock events used in this work are shown in two coordinate systems in Figure 2.2 with the trajectory of the spacecraft. The first coordinate system used is the heliocentric Earth ecliptic (HEE), in which the Earth is along the positive x-axis and z-axis is northward perpendicular to the ecliptic plane. The other coordinate system is the heliocentric Aries ecliptic (HAE), in which the x-axis instead points towards the first point of Aries. The HAE system is in inertial frame while HEE is not, which is explains the trajectory of the Solar orbiter in HEE system.

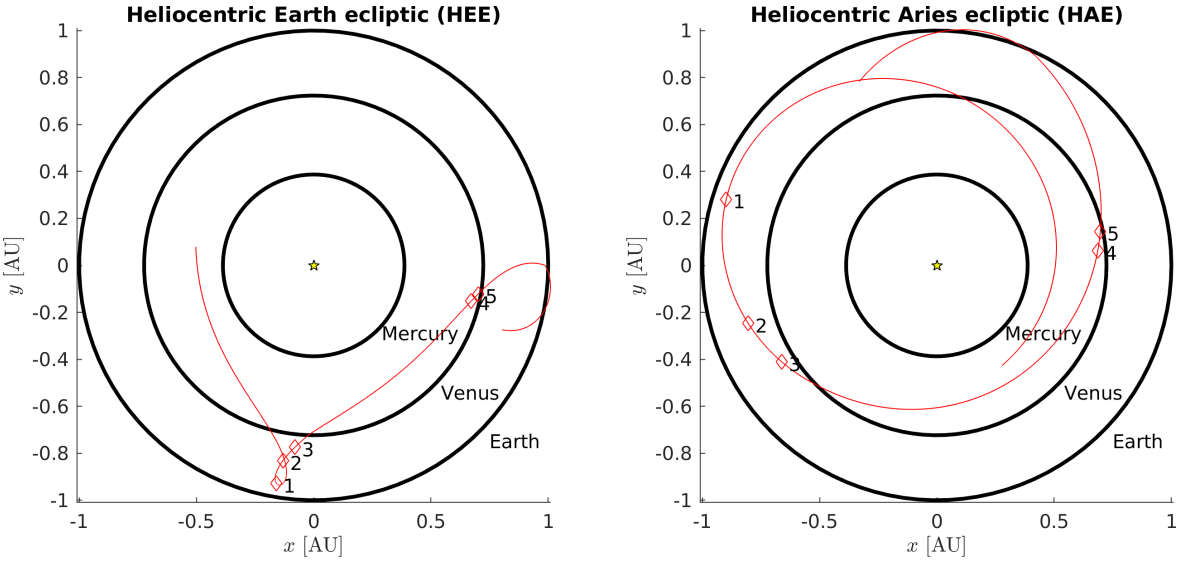

Figure 2.2: Location of the five Solar Orbiter shock crossings in two different heliocentric coordinate systems. Trajectory of the spacecraft from 2021-02-01 to 2022-02-01 is drawn as a red line with diamonds indicating the event locations. Approximate orbits of Earth, Venus and Mercury are drawn as black circles. The Sun is drawn as a yellow star.

At the time of the data, the solar cycle is near the solar minimum, causing there to be fewer shocks overall. The Solar Orbiter was launched in February 2020, very close

Table 2.1: All the Solar Orbiter events used in this work. R is the distance to the Sun at the time of the event.

	Time (UTC)	R [AU]
Event 1	2021-06-13 10:05	0.95
Event 2	2021-07-18 17:54	0.84
Event 3	2021-07-31 00:36	0.78
Event 4	2021-10-11 07:30	0.69
Event 5	2021-10-14 23:00	0.71

to the solar minimum*, but already there have been many shock events and we can expect an increasing amount as the solar cycle progresses toward to the solar maximum with time.

*Current solar cycle progression information taken from https://www.swpc.noaa.gov/products/solar-cycle-progression

3. Solar Orbiter shock crossings

3.1 Normal vector of an interplanetary shock

The determination of the normal vector of an interplanetary shock is not a trivial task as interplanetary shocks are relatively weak and pass past the observing spacecraft quick [Schwartz, 1998]. In this section we will go through different methods of determining the shock normal and compare the normal vectors produced by the different methods in the case of shock event 3 (see Table 2.1). This section is largely based on [Schwartz, 1998].

The magnetic field of a shock is coplanar, meaning it lies in the same plane both upstream and downstream of the shock. A number of vectors perpendicular to $\hat{\mathbf{n}}$ can be derived from this coplanarity which can be then used to calculate the normal vector

$$\hat{\mathbf{n}}_{mc} = \pm \frac{(\mathbf{B}_d \times \mathbf{B}_u) \times (\Delta \mathbf{B})}{|(\mathbf{B}_d \times \mathbf{B}_u) \times (\Delta \mathbf{B})|}, \tag{3.1}$$

where $\mathbf{B}_u$ and $\mathbf{B}_d$ is the upstream and downstream magnetic fields, respectively. $\Delta \mathbf{B} \equiv \mathbf{B}_d - \mathbf{B}_u$ is the jump in magnetic field at the shock. The terms upstream and downstream of a shock can get confusing in certain situations in interplanetary space. However, upstream and downstream correspond to the unshocked and shocked plasma respectively although we will continue to use the notation presented here. The magnetic coplanarity (MC) is easy to apply but fails when $\theta_{Bn} = 0°$ or $90°$.

Velocity is also subject to the same coplanarity resulting in

$$\hat{\mathbf{n}}_{vc} = \frac{\Delta V}{|\Delta V|}, \tag{3.2}$$

where ΔV is the change in velocity at the shock. Velocity coplanarity (VC) is only applicable when θ_{Bn} is close to $0°$ or $90°$, or when the Mach number is high which might not be the case in interplanetary shocks.

To account for the shortcomings of magnetic and velocity coplanarity methods a set of equations can be derived using both $\mathbf{B}$ and $\mathbf{V}$ to get three mixed method normal vectors

$$\hat{\mathbf{n}}_{mx1} = \pm \frac{(\mathbf{B}_u \times \boldsymbol{\Delta}\mathbf{V}) \times (\Delta \mathbf{B})}{|(\mathbf{B}_u \times \boldsymbol{\Delta}\mathbf{V}) \times (\Delta \mathbf{B})|}, \tag{3.3}$$

$$\hat{\mathbf{n}}_{mx2} = \pm \frac{(\mathbf{B}_d \times \mathbf{\Delta V}) \times (\Delta \mathbf{B})}{|(\mathbf{B}_d \times \mathbf{\Delta V}) \times (\Delta \mathbf{B})|}, \tag{3.4}$$

$$\hat{\mathbf{n}}_{mx3} = \pm \frac{(\mathbf{\Delta B} \times \mathbf{\Delta V}) \times (\Delta \mathbf{B})}{|(\mathbf{\Delta B} \times \mathbf{\Delta V}) \times (\Delta \mathbf{B})|}. \tag{3.5}$$

These mixed mode methods can give accurate estimates of the shock normal in most situations as long as data from particle instruments is available. While all three mixed modes work equally well, we will use mixed mode 3 as the main mixed mode.

Another method is the minimum variance analysis (MVAR) which aims to find the normal vector to a one dimensional wavefront from spacecraft data [Sonnerup and Scheible, 1998]. The normal vector $\hat{\mathbf{n}}_{mvar}$ is in the direction in which the magnetic field changes the least. Minimum variance analysis, along with magnetic coplanarity, only need $\mathbf{B}$ to estimate $\hat{\mathbf{n}}$, making them useful in a situation where plasma data is unavailable [e.g., Zhao et al., 2021]. In practice, $\hat{\mathbf{n}}_{mvar}$ can be determined by calculating eigenvectors and eigenvalues from the magnetic variance matrix

$$M^B_{\mu\nu} = \langle B_\mu B_\nu \rangle - \langle B_\mu \rangle \langle B_\nu \rangle \tag{3.6}$$

where $\mu, \nu = 1, 2, 3$ are the Cartesian components along the X, Y, Z system. The eigenvector $\mathbf{x_3}$ corresponds to the minimum variance and therefore the normal vector. The eigenvalue ratios can be used to test the quality of the minimum variance by calculating λ_2/λ_3 with the higher value meaning a more accurate result. Here, we will call this eigenvalue ratio the *quality value*.

Shock event 3 (Table 2.1) is shown in Figure 3.1. In this event, the shock is well defined fast forward shock where the magnetic field, number density and velocity jump up in the shock ramp, seen in the middle surrounded by the red region indicating the limits where the minimum variance is calculated. The region of the shock where upstream values $\mathbf{B}_u$ and $\mathbf{V}_u$ are calculated is colored with yellow whereas the downstream values are calculated in the blue region.

Table 3.1: The shock normal vector $\hat{\mathbf{n}}$ in all methods used in this work for event 3 (see Table 2.1)

Method	$\hat{\mathbf{n}}$	θ_{Bn} [°]
Mixed mode 3	(0.96, 0.03, 0.29)	59
Mixed mode 2	(0.94, 0.03, 0.34)	58
Mixed mode 1	(0.93, 0.03, 0.37)	58
Magnetic coplanarity	(0.76, 0.05, 0.65)	56
Velocity coplanarity	(0.89, 0.37, 0.25)	78
Minimum variance	(0.84, 0.39, 0.37)	78

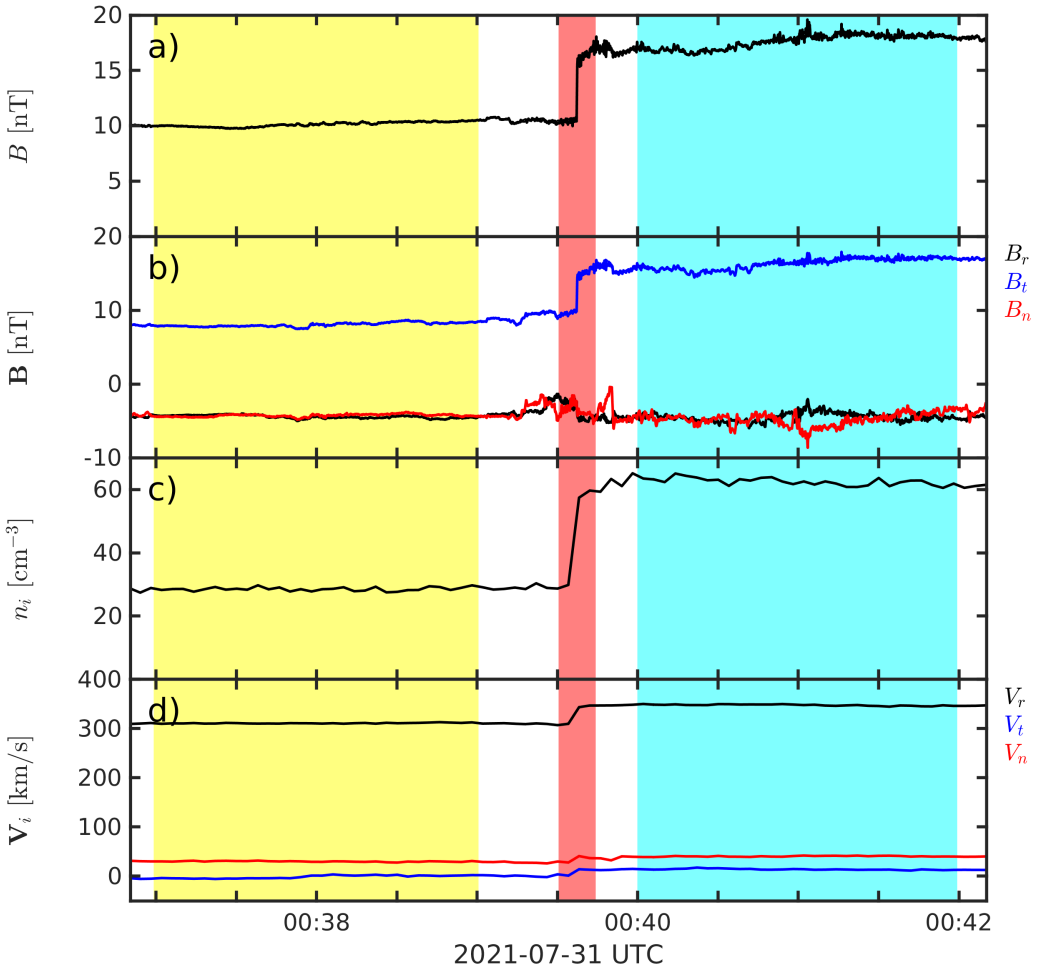

Figure 3.1: Properties of the shock event 3 (Table 2.1) in the RTN-coordinate system. Magnitude of the magnetic field, components of the magnetic field, number density and components of the velocity of the plasma are shown. Unshocked upstream plasma is shown in yellow and shocked downstream plasma is shown in blue. The region where minimum variance analysis is performed is marked with red.

The normal vectors for the event calculated with every method introduced in this section are shown in Table 3.1. The normal vectors are calculated in radial, tangential, normal (RTN) coordinate system, where the R-axis points radially outward from the Sun, the N is northward normal of the ecliptic plane and the T-axis is in the ecliptic plane and completes the right handed system. All the mixed mode methods produce similar normal vectors as expected, shown in Figure 3.2, with similar θ_{Bn} as well. The magnetic coplanarity method produced a similar θ_{Bn} even though $\hat{\mathbf{n}}_{mc}$ is 23° away from $\hat{\mathbf{n}}_{mx3}$. The velocity coplanarity and the minimum variance methods both have larger θ_{Bn} compared to the other methods as well as $\hat{\mathbf{n}}$ which are $\sim 20°$ away from $\hat{\mathbf{n}}_{mx3}$.

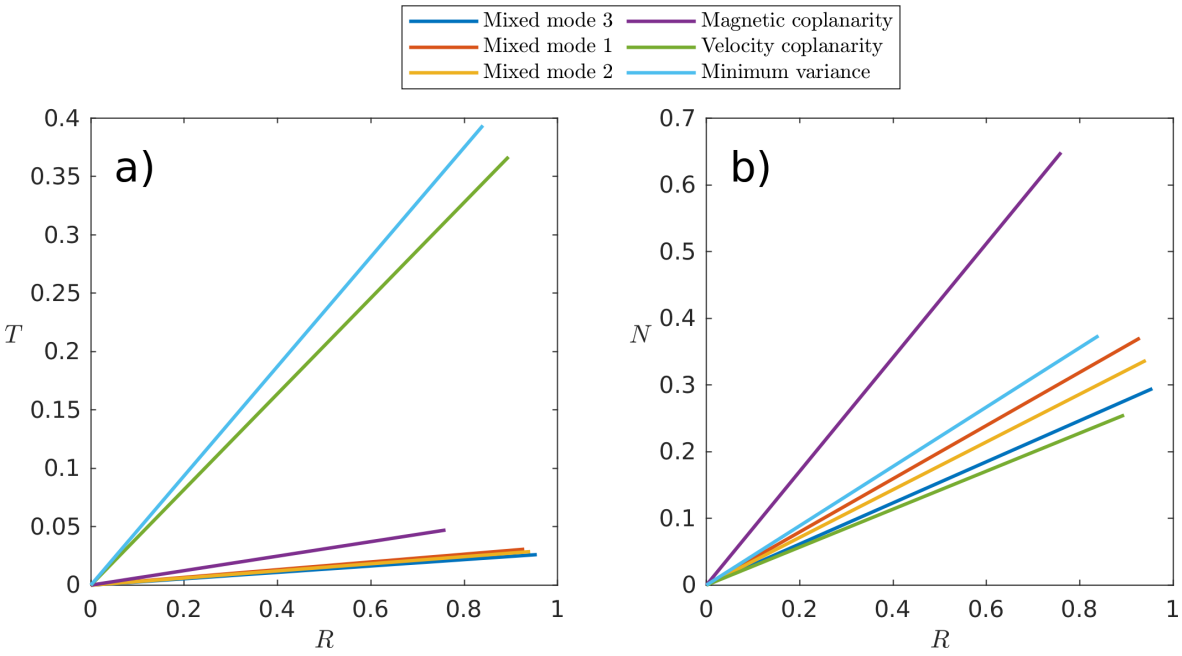

Figure 3.2: The calculated 3D shock normal vectors for event 3. RT-plane on the left and RN-plane on the right.

3.2 Comparing all events

So far we have inspected normal vector determination for one shock event. In this section we will go through all the events chosen for this work and compare the results of the different methods for determining $\hat{\mathbf{n}}$. We use mixed mode 3 as the assumed correct value for $\hat{\mathbf{n}}$ in the comparisons. All the previously unintroduced events are shown in Figure 3.3, with the selected unshocked upstream region colored with yellow, shocked downstream region with blue and the region for minimum variance with red. The events 1 and 4 are easily identifiable fast forward shocks whereas events 2 and 5 are more messy fast forward shocks. The magnetic field is rotating in event 2 with B_n changing sign before the shock. Because of this we do not expect $\hat{\mathbf{n}}$ from any method to be correct for this event. Event 5 has a chaotic upstream compared to the other events, probably due to lower shock angle θ_{Bn}, which we also see from our measurements (Table 3.2). This causes a hard to identify shock profile and also makes the determination of $\hat{\mathbf{n}}$ difficult and possibly inaccurate.

The different methods for determining $\hat{\mathbf{n}}$ are compared as an angle ϕ to $\hat{\mathbf{n}}_{mx3}$ for every event. These angles are shown in Table 3.3 while all $\hat{\mathbf{n}}_{mx3}$ can be seen in Table 3.2. The normal vectors for all events with all methods can be found in the Appendix in Table A.1. Since the vectors are 3D, the angles for different methods are only comparable to $\hat{\mathbf{n}}_{mx3}$, which means if the angle is similar between two methods, the actual vectors still may not be similar but are just at a similar 3D angle from $\hat{\mathbf{n}}_{mx3}$.

From the events, event 4 has the most similar normal vectors and unsurprisingly, event 5 has the largest variance in normal vectors as can be seen from the large ϕ angles.

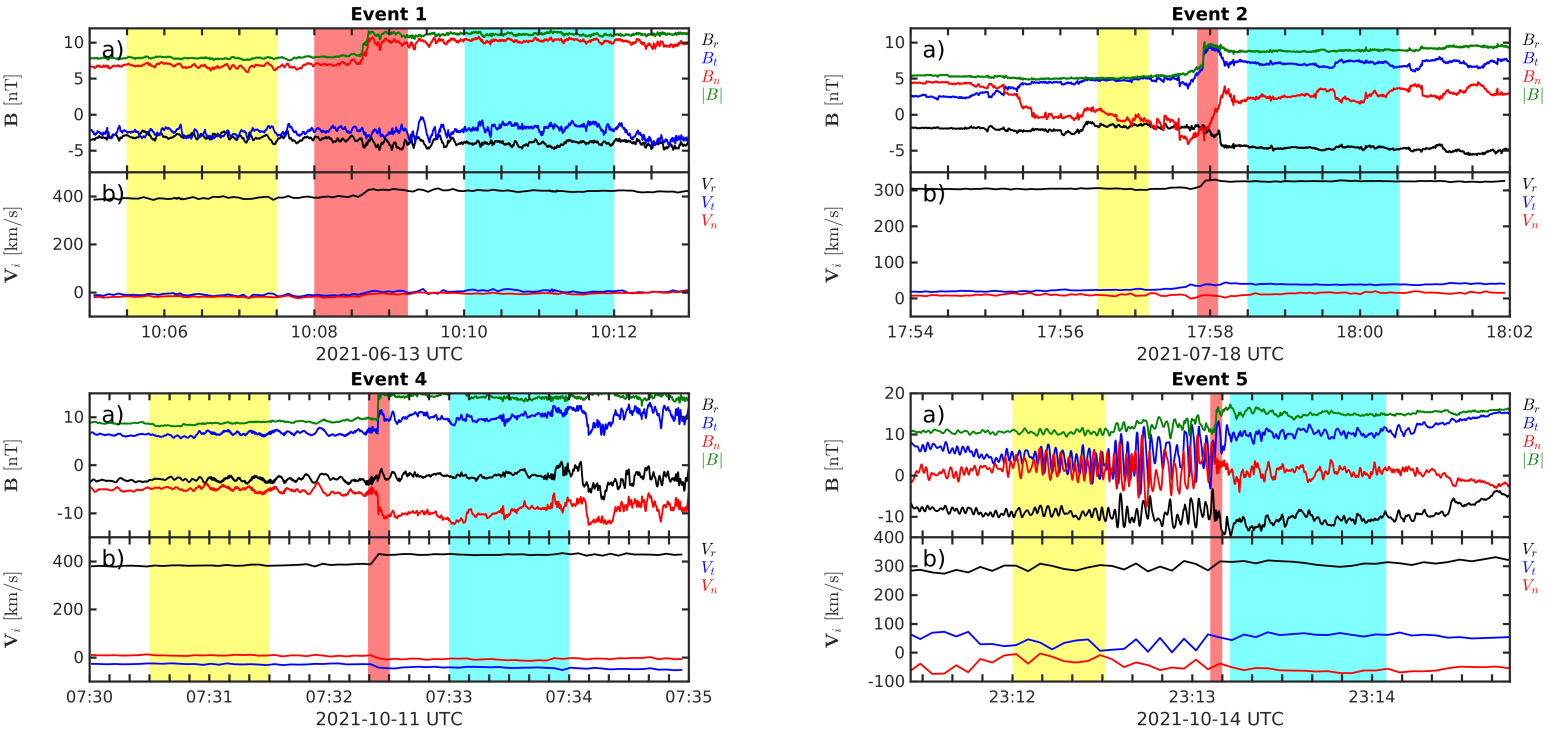

Figure 3.3: All shock events used in this work other than event 3 (Table 2.1). Components and magnitude of the magnetic field are shown in panel a and components of the velocity are shown in panel b for all events.

Table 3.2: $\hat{\mathbf{n}}_{mx3}$ for all events with angles between **B** and $\hat{\mathbf{n}}$, **B** and the Sun-Earth line, and $\hat{\mathbf{n}}$ and the Sun-Earth line

	$\hat{\mathbf{n}}_{mx3}$	θ_{Bn} [°]	θ_{Br} [°]	θ_{nr} [°]
Event 1	(0.91, 0.39, 0.15)	70	67	25
Event 2	(0.73, 0.62, 0.30)	70	73	43
Event 3	(0.96, 0.03, 0.30)	59	64	17
Event 4	(0.88, -0.45, -0.16)	57	70	28
Event 5	(0.56, -0.03, -0.83)	45	26	56

The mixed mode methods should in theory all be equally accurate. In the events used in this work, the mixed mode methods work well as ϕ_{mx2} is the smallest angle in every event with ϕ_{mx1} usually being second smallest. The velocity coplanarity generally results in normal vectors closer to $\hat{\mathbf{n}}_{mx3}$ than both methods using only magnetic field. Normal determination using only magnetic field results in large errors as can be seen from ϕ_{mc} and ϕ_{mvar} with the highest errors occurring with the magnetic coplanarity

method with $\phi_{mc} > 50°$ and the minimum variance method with $\phi_{mvar} > 30°$ in two events. The quality of the minimum variance method can be estimated using the ratio λ_2/λ_3 with higher being the best. This quality value is also shown in Table 3.3 for all events. Event 1 has $\lambda_2/\lambda_3 = 2.3$ which is usually considered poor while events 3 and 4 have λ_2/λ_3 between 4 and 5 which is considered okay in some studies and poor in others. Here, events 2 and 5 have the highest quality values but in event 2 ϕ_{mvar} is still large. This indicates that high value of the quality value does not indicate an accurate normal vector.

Table 3.3: The angle ϕ between $\hat{\mathbf{n}}_{mx3}$ (see Table 3.2) and other method $\hat{\mathbf{n}}$ vectors for all events. The quality value of minimum variance λ_2/λ_3 also shown for all events.

	Event 1	Event 2	Event 3	Event 4	Event 5
$\phi_{mx2}[°]$	3.5	3.7	2.6	0.0	11.7
$\phi_{mx1}[°]$	5.3	9.1	4.6	0.1	18.3
$\phi_{mc}[°]$	50.3	64.5	23.4	0.5	32.7
$\phi_{vc}[°]$	11.4	8.0	20.1	13.7	39.4
$\phi_{mvar}[°]$	33.8	30.2	22.7	9.8	12.4
λ_2/λ_3	2.3	16.9	4.2	4.9	14.2

Overall the mixed modes produce similar $\hat{\mathbf{n}}$ with $\phi < 10°$. The other methods deviate more from $\hat{\mathbf{n}}_{mx3}$ with the methods only using magnetic field having largest separation. Next, we will look into ways of validating our results with multi-spacecraft shock observations.

4. MMS event

The methods for determining the shock normal vector in this work are all single-spacecraft methods as Solar Orbiter is a single-spacecraft mission. While there are multi-spacecraft methods for determining the shock normal with far greater accuracy compared to single spacecraft methods, they are not in the scope of this project. We now look at one multi-spacecraft shock event observed by the Magnetospheric Multiscale (MMS) mission, see Figure 4.1. We calculate the normal vectors using the methods previously described in this work and compare them to the "real" normal vector calculated with multi-spacecraft timing method to test the validity of the single spacecraft methods.

The calculated shock normal vectors for all methods are shown in Table 4.1 with a timing method $\hat{\mathbf{n}}$ by Cohen et al. [2019]. The normal vectors are in Geocentric Solar Ecliptic (GSE) coordinate system which has the most notable difference to RTN-system in that the x-axis is reversed. The mixed mode methods provide the most accurate normal vectors to the timing method with the angle to the timing method $\hat{\mathbf{n}}$ being $\phi < 5°$. The velocity coplanarity is also very close to the mixed methods with less than a degree difference compared to mixed mode methods. For the minimum variance, we use the same time interval as [Hanson et al., 2019]. The resulting normal vector is slightly less accurate but still good with $\phi < 10°$. The quality value of the minimum variance is $\lambda_2/\lambda_3 = 5.5$. Clearly the worst of the methods is again the magnetic coplanarity with $\phi > 30°$. It is worth noting that the methods using only magnetic field in the determination (MC and MVAR) change a lot with different time intervals which raises uncertainty in the methods.

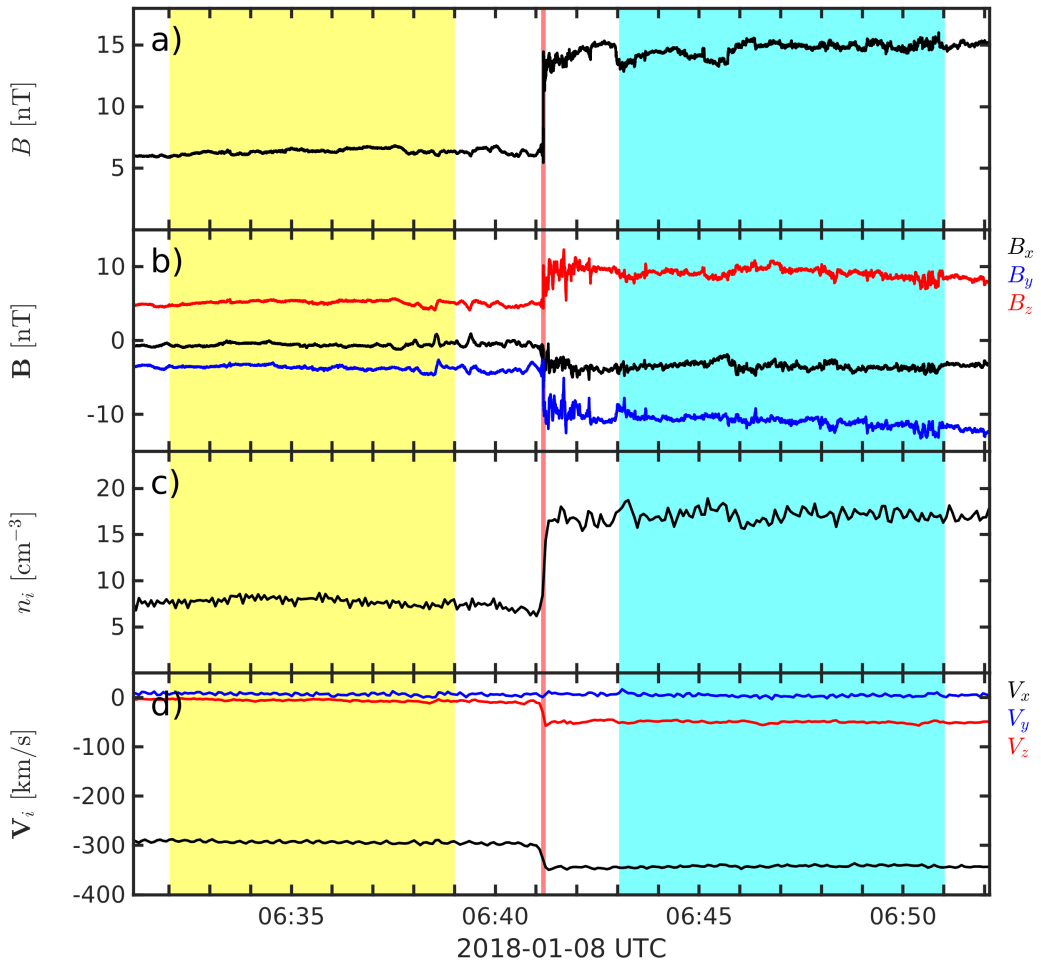

Figure 4.1: Interplanetary shock crossing observed by MMS1. Properties are in *GSE*-coordinate system. Magnitude of the magnetic field, components of the magnetic field, number density and components of the velocity of the plasma are shown. Unshocked upstream plasma is shown in yellow and shocked downstream plasma is shown in blue. The region where minimum variance analysis is performed is marked with red.

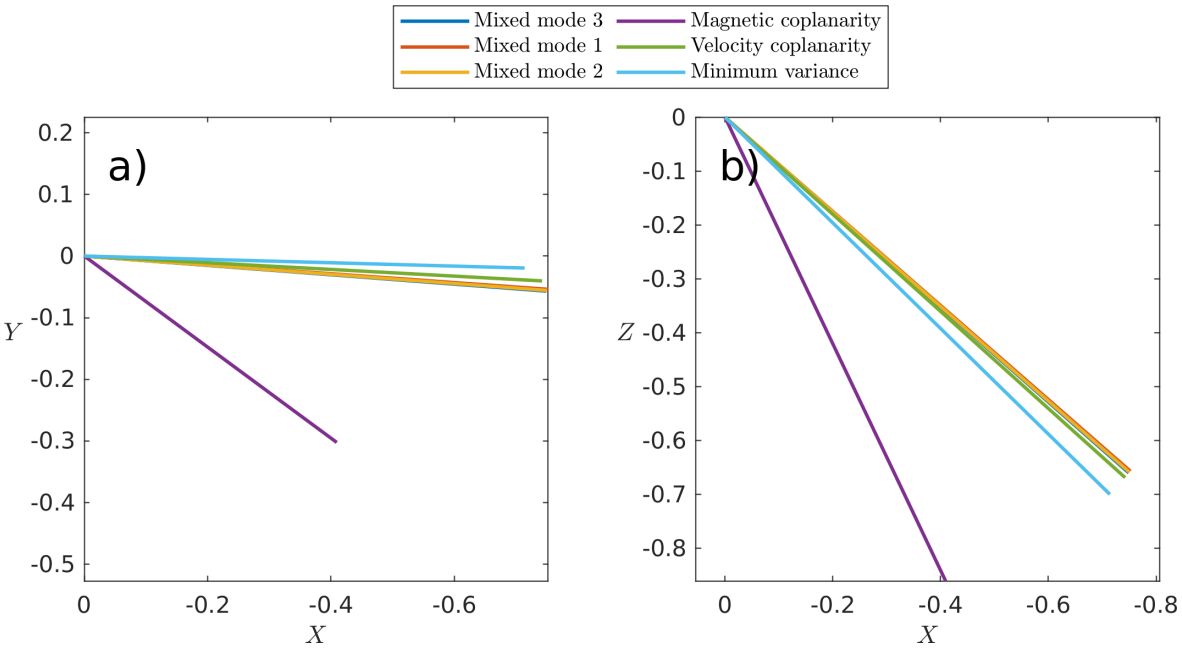

Figure 4.2: Calculated 3D shock normal vectors for the MMS event in *GSE*-coordinate system.

Table 4.1: Shock normal vectors with calculated angles ϕ between normal vectors of the multi-spacecraft timing method and other methods for the MMS event. θ_{Bn} shown for all methods. The angle between the upstream magnetic field and Sun-Earth line for this event is $\theta_{Br} = 85°$ and the angle between the shock normal and Sun-Earth line is $\theta_{nr} = 41°$. The quality value for minimum variance $\lambda_2/\lambda_3 = 5.5$

Method	$\hat{\mathbf{n}}$	$\phi[°]$	θ_{Bn} [°]
Timing [Cohen et al., 2019]	(-0.80, -0.04, -0.60)		67
Mixed mode 3	(-0.75, -0.06, -0.66)	4.9	64
Mixed mode 2	(-0.75, -0.06, -0.66)	4.8	64
Mixed mode 1	(-0.75, -0.05, -0.66)	4.6	64
Magnetic coplanarity	(-0.41, -0.30, -0.86)	31.5	60
Velocity coplanarity	(-0.74, -0.04, -0.86)	5.4	63
Minimum variance	(-0.71, -0.02, -0.70)	7.9	60

5. Conclusions

The purpose of this project was to test and compare different methods of determining the shock normal vector $\hat{\mathbf{n}}$ in interplanetary shock events observed by Solar Orbiter. A total of 5 shock events were studied, all of which were identified as shocks prior to this work. Events 2 and 5 have a more difficult shock profiles making the determination of $\hat{\mathbf{n}}$ harder. Event 5 has a messy upstream region upstream region and is therefore probably quasi-parallel shock, increasing the difficulty of normal determination. We used the magnetic and velocity coplanarity, 3 mixed mode and the minimum variance of the magnetic field method. After calculating the normal vectors with all methods for all events we compared the differences in the normal vectors assuming the mixed mode 3 method was the correct normal vector. Finally to validate the results, we studied one shock event observed by a multi-spacecraft mission MMS to compare the single spacecraft methods to the more accurate multi-spacecraft timing method.

We found that the methods using only magnetic field in the normal determination [Zhao et al., 2021], the magnetic coplanarity and minimum variance methods, were often very different from the mixed mode methods with the angle between the resulting normal vectors being sometimes over 30°. In some events, the quality value of the minimum variance λ_2/λ_3 was large (> 10) even though the normal vector was not accurate, suggesting the quality value is not a good indicator of an accurate normal estimation at interplanetary shocks. The velocity coplanarity provided better normal vectors compared to magnetic field methods, but still not as good as the mixed mode methods. As it is rare to have observations with plasma data without magnetic field data, the velocity coplanarity is rarely useful as one could use mixed mode methods instead.

To validate our results we calculated the normal vectors for a shock event observed by MMS, which is a multi-spacecraft mission capable of determining the shock normal with greater accuracy compared to single-spacecraft methods. The results were consistent with the previously studied events with the mixed mode methods being the closest to the "real" normal vector even though they had deviated by $\sim 5°$.

In this work we have shown that plasma data, like flow velocity, are necessary for the determination of shock normal vector at interplanetary shocks using Solar Orbiter.

In future work more methods could be investigated such as the maximum variance of the electric field at the shock [Hanson et al., 2019]. The accuracy of the determination of additional shock parameters such as the shock speed and Mach number using different methods could also be investigated.

Acknowledgements

Thank you to my supervisor Andreas Johlander at IRF Uppsala for guidance and comments throughout the project. Thank you to the examiner of this project Markus Battarbee. Finally, I would like to thank Andrew Dimmock at IRF for identifying and providing the Solar Orbiter interplanetary shock events used here. The SolO data used in this work are available at the Solar Orbiter Archive https://soar.esac.esa.int/soar/.

Appendix A. Shock normal vectors for all Solar Orbiter events

Table A.1: All $\hat{\mathbf{n}}$ for all Solar Orbiter events.

	Event 1	Event 2	Event 3	Event 4	Event 5
$\hat{\mathbf{n}}_{mx3}$	(0.91, 0.39, 0.15)	(0.73, 0.62, 0.30)	(0.96, 0.03, 0.29)	(0.88, -0.45, -0.16)	(0.56, -0.03, -0.83)
$\hat{\mathbf{n}}_{mx2}$	(0.89, 0.44, 0.13)	(0.71, 0.66, 0.25)	(0.94, 0.03, 0.34)	(0.88, -0.45, -0.16)	(0.71, 0.04, -0.71)
$\hat{\mathbf{n}}_{mx1}$	(0.87, 0.47, 0.12)	(0.68, 0.71, 0.18)	0.93, 0.03, 0.37)	(0.88, -0.45, -0.16)	(0.78, 0.08, -0.62)
$\hat{\mathbf{n}}_{mc}$	(0.32, 0.94, -0.13)	(0.10, 0.84, -0.53)	(0.76, 0.05, 0.65)	(0.88, -0.45, -0.17)	(0.89, 0.16, -0.42)
$\hat{\mathbf{n}}_{vc}$	(0.84, 0.42, 0.34)	(0.81, 0.55, 0.21)	(0.89, 0.37, 0.25)	(0.89, -0.29, -0.34)	(0.26, 0.57, -0.78)
$\hat{\mathbf{n}}_{mvar}$	(0.53, 0.82, 0.23)	(0.95, 0.15, 0.26)	(0.84, 0.39, 0.37)	(0.79, -0.58, -0.21)	(0.46, -0.22, -0.86)

Bibliography

L. F. Burlaga. Interplanetary magnetohydrodynamics. *Interplanetary magnetohydrodynamics*, 3, Jan. 1995.

L. F. Burlaga, N. F. Ness, M. H. Acuña, J. D. Richardson, E. Stone, and F. B. McDonald. Observations of the Heliosheath and Solar Wind Near the Termination Shock by Voyager 2. ApJ, 692(2):1125–1130, Feb. 2009. doi: 10.1088/0004-637X/692/2/1125.

I. J. Cohen, S. J. Schwartz, K. A. Goodrich, N. Ahmadi, R. E. Ergun, S. A. Fuselier, M. I. Desai, E. R. Christian, D. J. McComas, G. P. Zank, J. R. Shuster, S. K. Vines, B. H. Mauk, R. B. Decker, B. J. Anderson, J. H. Westlake, O. Le Contel, H. Breuillard, B. L. Giles, R. B. Torbert, and J. L. Burch. High-Resolution Measurements of the Cross-Shock Potential, Ion Reflection, and Electron Heating at an Interplanetary Shock by MMS. *Journal of Geophysical Research (Space Physics)*, 124(6):3961–3978, June 2019. doi: 10.1029/2018JA026197.

D. B. Guenther, P. Demarque, Y. C. Kim, and M. H. Pinsonneault. Standard Solar Model. ApJ, 387:372, Mar. 1992. doi: 10.1086/171090.

E. L. M. Hanson, O. V. Agapitov, F. S. Mozer, V. Krasnoselskikh, S. D. Bale, L. Avanov, Y. Khotyaintsev, and B. Giles. Cross-Shock Potential in Rippled Versus Planar Quasi-Perpendicular Shocks Observed by MMS. Geophys. Res. Lett., 46(5): 2381–2389, Mar. 2019. doi: 10.1029/2018GL080240.

T. S. Horbury, H. O'Brien, I. Carrasco Blazquez, M. Bendyk, P. Brown, R. Hudson, V. Evans, T. M. Oddy, C. M. Carr, T. J. Beek, E. Cupido, S. Bhattacharya, J. A. Dominguez, L. Matthews, V. R. Myklebust, B. Whiteside, S. D. Bale, W. Baumjohann, D. Burgess, V. Carbone, P. Cargill, J. Eastwood, G. Erdös, L. Fletcher, R. Forsyth, J. Giacalone, K. H. Glassmeier, M. L. Goldstein, T. Hoeksema, M. Lockwood, W. Magnes, M. Maksimovic, E. Marsch, W. H. Matthaeus, N. Murphy, V. M. Nakariakov, C. J. Owen, M. Owens, J. Rodriguez-Pacheco, I. Richter, P. Riley, C. T. Russell, S. Schwartz, R. Vainio, M. Velli, S. Vennerstrom, R. Walsh, R. F. Wimmer-

Schweingruber, G. Zank, D. Müller, I. Zouganelis, and A. P. Walsh. The Solar Orbiter magnetometer. A&A, 642:A9, Oct. 2020. doi: 10.1051/0004-6361/201937257.

S. M. Krimigis, R. B. Decker, M. E. Hill, T. P. Armstrong, G. Gloeckler, D. C. Hamilton, L. J. Lanzerotti, and E. C. Roelof. Voyager 1 exited the solar wind at a distance of ∼85AU from the Sun. Nature, 426(6962):45–48, Nov. 2003. doi: 10.1038/nature02068.

M. P. Miralles and J. Sánchez Almeida. *The Sun, the Solar Wind, and the Heliosphere*, volume 4. Springer Dordrecht, 2011. doi: 10.1007/978-90-481-9787-3.

D. Müller, O. C. St. Cyr, I. Zouganelis, H. R. Gilbert, R. Marsden, T. Nieves-Chinchilla, E. Antonucci, F. Auchère, D. Berghmans, T. S. Horbury, R. A. Howard, S. Krucker, M. Maksimovic, C. J. Owen, P. Rochus, J. Rodriguez-Pacheco, M. Romoli, S. K. Solanki, R. Bruno, M. Carlsson, A. Fludra, L. Harra, D. M. Hassler, S. Livi, P. Louarn, H. Peter, U. Schühle, L. Teriaca, J. C. del Toro Iniesta, R. F. Wimmer-Schweingruber, E. Marsch, M. Velli, A. De Groof, A. Walsh, and D. Williams. The Solar Orbiter mission. Science overview. A&A, 642:A1, Oct. 2020. doi: 10.1051/0004-6361/202038467.

C. J. Owen, R. Bruno, S. Livi, P. Louarn, K. Al Janabi, F. Allegrini, C. Amoros, R. Baruah, A. Barthe, M. Berthomier, S. Bordon, C. Brockley-Blatt, C. Brysbaert, G. Capuano, M. Collier, R. DeMarco, A. Fedorov, J. Ford, V. Fortunato, I. Fratter, A. B. Galvin, B. Hancock, D. Heirtzler, D. Kataria, L. Kistler, S. T. Lepri, G. Lewis, C. Loeffler, W. Marty, R. Mathon, A. Mayall, G. Mele, K. Ogasawara, M. Orlandi, A. Pacros, E. Penou, S. Persyn, M. Petiot, M. Phillips, L. Přech, J. M. Raines, M. Reden, A. P. Rouillard, A. Rousseau, J. Rubiella, H. Seran, A. Spencer, J. W. Thomas, J. Trevino, D. Verscharen, P. Wurz, A. Alapide, L. Amoruso, N. André, C. Anekallu, V. Arciuli, K. L. Arnett, R. Ascolese, C. Bancroft, P. Bland, M. Brysch, R. Calvanese, M. Castronuovo, I. Čermák, D. Chornay, S. Clemens, J. Coker, G. Collinson, R. D'Amicis, I. Dandouras, R. Darnley, D. Davies, G. Davison, A. De Los Santos, P. Devoto, G. Dirks, E. Edlund, A. Fazakerley, M. Ferris, C. Frost, G. Fruit, C. Garat, V. Génot, W. Gibson, J. A. Gilbert, V. de Giosa, S. Gradone, M. Hailey, T. S. Horbury, T. Hunt, C. Jacquey, M. Johnson, B. Lavraud, A. Lawrenson, F. Leblanc, W. Lockhart, M. Maksimovic, A. Malpus, F. Marcucci, C. Mazelle, F. Monti, S. Myers, T. Nguyen, J. Rodriguez-Pacheco, I. Phillips, M. Popecki, K. Rees, S. A. Rogacki, K. Ruane, D. Rust, M. Salatti, J. A. Sauvaud, M. O. Stakhiv, J. Stange, T. Stubbs, T. Taylor, J. D. Techer, G. Terrier, R. Thibodeaux, C. Urdiales, A. Varsani, A. P. Walsh, G. Watson, P. Wheeler, G. Willis, R. F. Wimmer-Schweingruber, B. Winter,

J. Yardley, and I. Zouganelis. The Solar Orbiter Solar Wind Analyser (SWA) suite. A&A, 642:A16, Oct. 2020. doi: 10.1051/0004-6361/201937259.

H. Porsche. HELIOS mission: Mission objectives, mission verification, selected results. In W. R. Burke, editor, *Solar System and its Exploration*, volume 164 of *ESA Special Publication*, pages 43–50, Nov. 1981.

J. D. Richardson. Shocks and sheaths in the heliosphere. *Journal of Atmospheric and Solar-Terrestrial Physics*, 73(11-12):1385–1389, July 2011. doi: 10.1016/j.jastp.2010.06.005.

S. J. Schwartz. Shock and Discontinuity Normals, Mach Numbers, and Related Parameters. *ISSI Scientific Reports Series*, 1:249–270, 1998.

R. Schwenn and E. Marsch. *Physics of the Inner Heliosphere I. Large-Scale Phenomena.* Springer Berlin, Heidelberg, 1990. doi: 10.1007/978-3-642-75361-9.

B. U. Ö. Sonnerup and M. Scheible. Minimum and Maximum Variance Analysis. *ISSI Scientific Reports Series*, 1:185–220, Jan. 1998.

K. P. Wenzel, R. G. Marsden, D. E. Page, and E. J. Smith. The ULYSSES Mission. A&AS, 92:207, Jan. 1992.

L. L. Zhao, G. P. Zank, J. S. He, D. Telloni, Q. Hu, G. Li, M. Nakanotani, L. Adhikari, E. K. J. Kilpua, T. S. Horbury, H. O'Brien, V. Evans, and V. Angelini. Turbulence and wave transmission at an ICME-driven shock observed by the Solar Orbiter and Wind. A&A, 656:A3, Dec. 2021. doi: 10.1051/0004-6361/202140450.